

# Non-Newtonian effects of blood flow on hemodynamics in distal vascular graft anastomoses

Jie Chen<sup>a</sup>, Xi-Yun Lu<sup>a,\*</sup>, Wen Wang<sup>b</sup>

<sup>a</sup>*Department of Modern Mechanics, University of Science and Technology of China, Hefei, Anhui 230026, PR China*

<sup>b</sup>*Medical Engineering Division, Department of Engineering, Queen Mary, University of London, London E1 4NS, UK*

Accepted 16 June 2005

## Abstract

Non-Newtonian fluid flow in a stenosed coronary bypass is investigated numerically using the Carreau–Yasuda model for the shear thinning behavior of the blood. End-to-side coronary bypass anastomosis is considered in a simplified model geometry where the host coronary artery has a 75% severity stenosis. Different locations of the bypass graft to the stenosis and different flow rates in the graft and in the host artery are studied. Particular attention is given to the non-Newtonian effect of the blood on the primary and secondary flow patterns in the host coronary artery and the wall shear stress (WSS) distribution there. Interaction between the jet flow from the stenosed artery and the flow from the graft is simulated by solving the three-dimensional Navier–Stokes equation coupled with the non-Newtonian constitutive model. Results for the non-Newtonian flow, the Newtonian flow and the rescaled Newtonian flow are presented. Significant differences in axial velocity profiles, secondary flow streamlines and WSS between the non-Newtonian and Newtonian fluid flows are revealed. However, reasonable agreement between the non-Newtonian and the rescaled Newtonian flows is found. Results from this study support the view that the residual flow in a partially occluded coronary artery interacts with flow in the bypass graft and may have significant hemodynamic effects in the host vessel downstream of the graft. Non-Newtonian property of the blood alters the flow pattern and WSS distribution and is an important factor to be considered in simulating hemodynamic effects of blood flow in arterial bypass grafts.

© 2005 Elsevier Ltd. All rights reserved.

*Keywords:* Non-Newtonian fluid flow; Stenosis; Coronary bypass; Wall shear stress; Numerical simulation

## 1. Introduction

Anastomotic intimal hyperplasia and thrombosis are often implicated in the failure of coronary bypass surgery. In vivo animal models reveal that the heel, toe, suture-line and the artery wall opposite to the junction are most prone to intimal thickening (Imparato et al., 1972; Sottiurai et al., 1989). Several initiating factors have been speculated in the pathogenesis of the intimal thickening, one of which is the local variation in the wall shear stress (WSS) (Cole et al., 1998; Ethier

et al., 1998; Perktold et al., 1998). In vitro experiments have been carried out to measure velocity distribution and to visualize flow pattern in end-to-side anastomosis (Crawshaw et al., 1980; Rittgers et al., 1978; Keynton et al., 1991). Hemodynamic effects of the blood flow are believed to play an important role in the initiation and development of the intimal thickening following coronary bypass surgery (Caro et al., 1971; Friedman et al., 1981; Zarins et al., 1983; Nerem, 1992). There have been a number of theoretical studies on Newtonian flow in bypass grafts (e.g., Perktold et al., 1998; Lee et al., 2001; Lu et al., 2002). Rheological properties of the blood, which may affect significantly local hemodynamics, however, have not been rigorously investigated in end-to-side coronary bypass anastomosis (Thurston, 1973, 1979; Chen and Lu, 2004, 2005).

\*Corresponding author. Tel.: +86 551 3603223;  
fax: +86 551 3606459.

E-mail address: xlu@ustc.edu.cn (X.-Y. Lu).

Numerical simulation is an important tool in investigating blood flow in arteries. Previous studies investigated unsteady blood flow (e.g., Tu and Deville, 1996), in three-dimensional (3D) geometries (e.g., Hofer et al., 1996; Santamarina et al., 1998; Weydahl and Moore Jr., 2001), and in 3D geometries reconstructed from arteries using data from experiments (e.g., Friedman and Ding, 1998; Perktold et al., 1998). The influence of the angle of the anastomosis and flow divisions in models of artery bypass on the WSS and flow patterns has been studied extensively (e.g., Fei et al., 1994; Henry et al., 1996; Inzoli et al., 1996; Bertolotti and Deplano, 2000; Bertolotti et al., 2001). Non-Newtonian effects of blood flow in arterial bifurcations were also considered (e.g., Lou and Yang, 1993; Gijssen et al., 1999a, b; Chen and Lu, 2004, 2005).

In this study, steady non-Newtonian flow in a simplified geometry for coronary bypass is simulated under different flow conditions and graft locations. The 3D Navier–Stokes equations coupled with the non-Newtonian constitutive model are solved numerically using a finite element method. To compare the flow behavior of the non-Newtonian fluid with that of the Newtonian fluid, results for the Newtonian fluid with the original Reynolds number and the rescaled Reynolds number are calculated. Interaction between the flow from the bypass graft and the flow from the partially occluded host artery is investigated, when anastomosis is at different distances to the site of the stenosis. The emphasis of the study is on the primary and secondary flows and WSS distribution in the host artery downstream of the bypass graft, and how non-Newtonian effects of the blood affect these distributions.

**2. Methods**

The flow is assumed to be steady and laminar. Governing equations for an incompressible fluid, i.e., Navier–Stokes equations, are

$$\rho \left( \frac{\partial \mathbf{u}}{\partial t} + \mathbf{u} \cdot \nabla \mathbf{u} \right) = -\nabla p + \nabla \cdot \mathbf{T}, \tag{1}$$

$$\nabla \cdot \mathbf{u} = 0, \tag{2}$$

where  $\mathbf{u}$  is the fluid velocity vector,  $\rho$  the density and  $p$  the pressure.  $\mathbf{T}$  is the stress tensor and is linearly dependent on the rate of deformation tensor  $\mathbf{D}$  with a relation of  $\mathbf{T} = 2\eta(\dot{\gamma})\mathbf{D}$ , where  $\mathbf{D} = \frac{1}{2}(\nabla \mathbf{u} + \nabla \mathbf{u}^T)$ ,  $\eta$  represents the viscosity of the blood, and  $\dot{\gamma}$  is the shear rate. For a non-Newtonian fluid,  $\eta$  is a function of  $\dot{\gamma}$ , and for a Newtonian fluid  $\eta$  is a constant and is independent of the shear rate  $\dot{\gamma}$ .

The shear thinning and viscoelasticity of the blood are related to its microscopic structures and are determined mainly by red blood cells in the blood, e.g., aggregation,

deformation and alignment of red blood cells (Chien et al., 1970; Thurston, 1973, 1979). Studies on the steady non-Newtonian flow in a carotid bifurcation model indicate that the shear thinning is the dominant non-Newtonian property of the blood affecting the velocity distribution (Gijssen et al., 1999a, b), although viscoelasticity of the blood has been demonstrated to affect flow patterns (Liesch and Moravec, 1984; Ku and Liesch, 1986). In the present study, the Carreau–Yasuda shear thinning model (Bird et al., 1987) was used,

$$\frac{\eta - \eta_\infty}{\eta_0 - \eta_\infty} = [1 + (\lambda\dot{\gamma})^a]^{(n-1)/a}, \tag{3}$$

where  $\dot{\gamma}$  represents a scalar quantity of the rate of deformation tensor, defined as  $\dot{\gamma} = \sqrt{2\text{tr}(\mathbf{D}^2)}$ . The other parameters in Eq. (3) are employed from the experimental data based on the analog blood fluid (Gijssen et al., 1999a, b) and written as  $\eta_\infty = 2.2 \times 10^{-3}$  Pa s,  $\eta_0 = 22 \times 10^{-3}$  Pa s,  $\lambda = 0.110$  s,  $a = 0.644$ ,  $n = 0.392$  and  $\rho = 1410$  kg/m<sup>3</sup>.

As shown in Fig. 1, a simplified anastomosis model is represented as the intersection of two cylinders with the

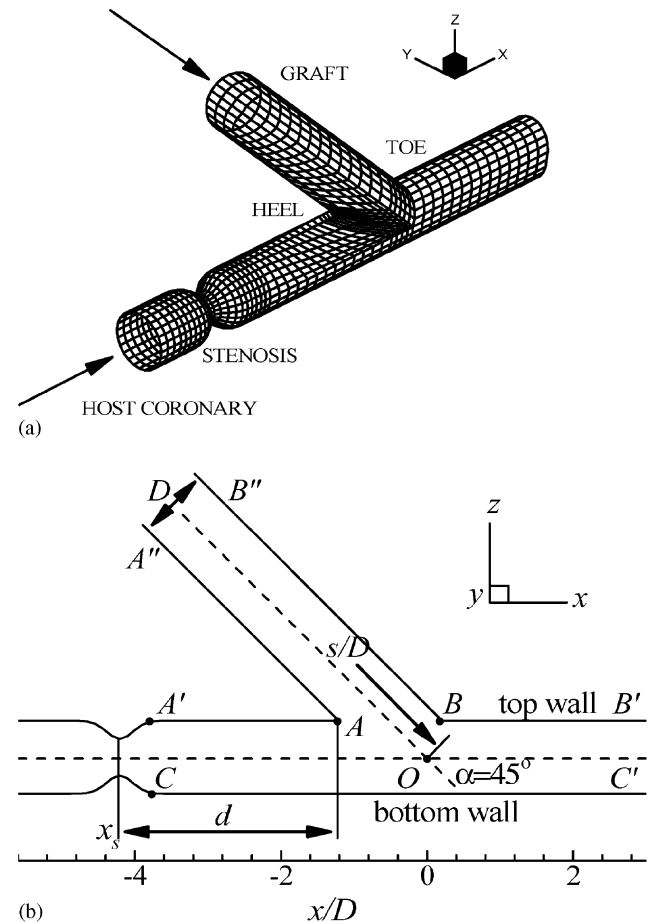


Fig. 1. Schematic drawing of a distal vascular anastomosis. The bypass graft has the same diameter,  $D$ , as the host artery. The distance between the heel of the graft and the center of the stenosis is  $d$ . (a) Global view; (b) view in the  $x$ – $z$  plane of symmetry.

same diameter  $D$  at a junction angle of  $45^\circ$ . As reported by Ofili et al. (1995), the diameter of the left anterior descending coronary is approximately 3 mm (i.e.,  $D = 3$  mm). A 75% lumen axisymmetric stenosis is considered and is described by a Gaussian profile (Siouff et al., 1998),

$$\frac{R(x)}{R_0} = 1 - \frac{1}{2} \exp\left(-\frac{4(x - x_s)^2}{R_0^2}\right), \quad (4)$$

where  $R(x)$  is the radius of the constricted part in the host coronary with  $R_0 = 1.5$  mm,  $x_s$  represents the position of stenosis. The stenosis takes different positions upstream from the heel (in Fig. 1b):  $d = 1.5D$ ,  $2D$  and  $3D$ , and for easy reference in following sections, they are denoted as cases  $D1.5$ ,  $D2$  and  $D3$ , respectively. The case without stenosis is referred to as  $D0$ .

In order to compare results between the non-Newtonian and Newtonian flows, calculations were also performed using the Newtonian fluid employed by Gijsen et al. (1999b). Based on the experimental data of the analog blood fluid (Gijsen et al., 1999a, b), a concentrated solution of potassium thiocyanate in water (KSCN, 71% by weight) was employed as the Newtonian control fluid with the Newtonian viscosity  $\eta = 2.9 \times 10^{-3}$  Pa s. In the calculation, a typical Reynolds number,  $Re = 250$ , is used for the steady arterial flow. Based on the diameter of the host coronary artery ( $D = 3$  mm), the fluid density ( $\rho = 1410$  kg/m<sup>3</sup>) and viscosity ( $\eta = 2.9 \times 10^{-3}$  Pa s), the mean velocity at the outlet of the host artery is approximately 0.1714 m/s and the flow rate  $Q = 1.708 \times 10^{-3}$  kg/s.

To understand the equivalent viscous behavior of blood circulation in the host artery, a rescaled Newtonian flow is introduced. In order to define the corresponding rescaled Reynolds number, a characteristic shear rate (i.e.,  $\dot{\gamma}_c$ ) is needed. Different definitions of the characteristic shear rate for the blood flow in large arteries exist. Some use the wall shear rate (e.g., Mann and Tarbell, 1990; Cho and Kensey, 1991), which is often the highest shear rate occurring in blood flow. Others use the averaged shear rate in the artery (e.g., Thurston, 1973, 1979; Baaijens et al., 1993; Ballyk et al., 1994; Gijsen et al., 1999b; Chen and Lu, 2004, 2005). In this study, the averaged shear rate at the outlet of the host artery is used,

$$\dot{\gamma}_c = \frac{2V}{R_0}, \quad (5)$$

where  $V$  and  $R_0$  represent the mean velocity at the outlet and the radius of the host coronary tube, respectively. Based on the mean velocity of 0.1714 m/s and host diameter of 3 mm, the averaged shear rate is  $228.5$  s<sup>-1</sup>. From Eq. (3), with parameters by Gijsen et al. (1999a, b), the equivalent viscosity is approximately  $4.7 \times 10^{-3}$  Pa s. The rescaled Reynolds number is

Table 1  
Flow rates in bypass graft and in the stenosed host artery

Case reference	Flow rate in graft	Flow rate in host artery
$Q_{12}$	$Q/2$	$Q/2$
$Q_{34}$	$3Q/4$	$Q/4$
$Q_{78}$	$7Q/8$	$Q/8$

estimated to be 154.5, based on  $D = 3$  mm,  $\rho = 1410$  kg/m<sup>3</sup>, and the mean velocity of 0.1714 m/s.

As in previous studies (Weydahl and Moore Jr., 2001; Lu et al., 2002; Chen and Lu, 2004, 2005), fully developed velocity profiles are imposed at the two inlet sections (i.e., graft and host coronary). The residual blood flow in the constricted artery progressively decreases during the weeks following the surgery until the stenosed vessel is completely occluded (Kakos et al., 1972). Three different ratios between flow rates in the graft and in the host artery are used to simulate different hemodynamic conditions, as listed in Table 1 (Bertolotti and Deplano, 2000). The outflow boundary conditions are treated as a traction-free surface, and imposed  $20D$  downstream from the anastomosis in order to avoid perturbations in the upstream flow field. Vessels are assumed to be rigid and no-slip velocity condition is applied on the vessel walls.

A finite element method based on the fractional-step velocity correction is used to solve Eqs. (1) and (2) numerically. The finite element spatial discretization is performed using the Galerkin weighted residual method. The discretized formulation was described by Kovacs and Kawahara (1991) in detail. The computational method has been validated in our previous studies for Newtonian and non-Newtonian fluid flows in a non-planar bifurcation model (Lu et al., 2002; Chen and Lu, 2004, 2005). To validate the computational method in the anastomosis model, axial velocity profiles of the Newtonian flow in the symmetry plane (i.e.,  $x - z$  plane) are calculated and compared to data obtained by Bertolotti and Deplano (2000) in Fig. 2. Good agreement between the two results is seen for both  $D1.5$  and  $D0$  cases, when the flow in the bypass graft is  $\frac{1}{2}$ ,  $\frac{3}{4}$  and  $\frac{7}{8}$  of the total flow, i.e.,  $Q_{12}$ ,  $Q_{34}$  and  $Q_{78}$ .

### 3. Results

#### 3.1. Velocity profiles

Near the anastomosis, flow pattern is complex and is related to the initiation and development of intimal thickening (Imparato et al., 1972; Sottiurati et al., 1989). The change in the flow direction from the graft to the host vessel causes flow distortion due to the centrifugal force and the transverse pressure gradient

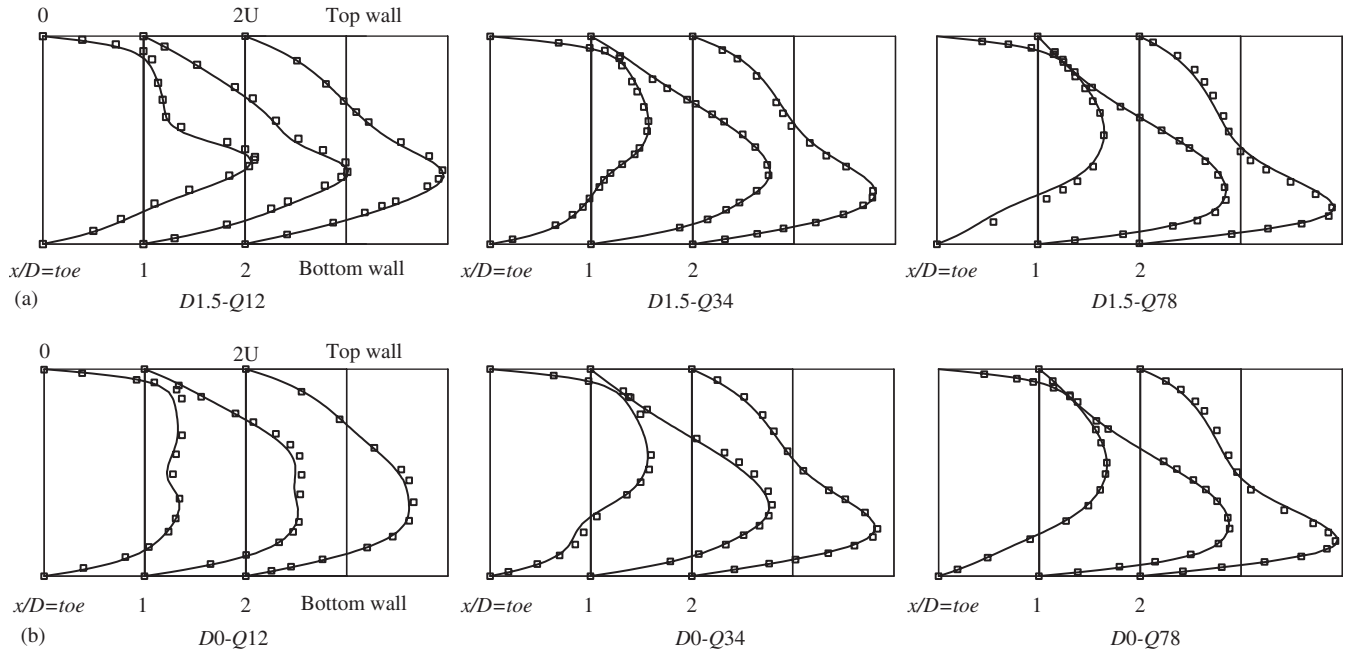


Fig. 2. Validation of the numerical method by axial velocity profiles in the symmetry plane. The ratio between flows in the stenosed artery and in the bypass graft takes different values. Symbol  $\square$  denotes data by Bertolotti and Deplano (2000) and solid line is for result from the present study. (a) With stenosis (D1.5); (b) without stenosis (D0).

in the cross-sectional plane. In addition, the residual flow from the stenosed artery creates a jet flow interacting with the flow from the graft. Fig. 3 shows the development of the axial velocity profiles in the symmetry plane (i.e., the  $x - z$  plane) from the toe to two vessel diameters downstream in the host artery. It is found that in the region near the toe, axial flow is significantly influenced by the interaction between the jet flow from the stenosed artery and that from the graft. At the toe, the peak velocity shifts toward the centerline of the artery as the flow rate in the graft increases, i.e., from Q12 to Q34 and Q78, for both the Newtonian and non-Newtonian flows. The jet flow from the stenosed artery tends to increase the peak value of the axial velocity, especially at D1.5–Q12 in Fig. 3a where the stenosis is closest to the anastomosis and flow rate in the stenosed artery equals that in the bypass graft. The jet effect reduces as the distance  $x/D$  increases, i.e., from D1.5 to D3 and D0, where the location of the stenosis can be viewed as infinitely far away from the heel at D0. Meanwhile, as the coronary inflow decreases (e.g., at Q34, Q78), the influence of the jet flow is hardly noticeable at the toe, particularly as the distance of the stenosis increases (e.g., D2, D3, or D0). At sections downstream of the toe, the axial velocity profiles are clearly skewed toward the bottom wall of the artery. The peak velocity is closer to the bottom wall as the flow rate in the graft increases (e.g., from Q1/2 to Q34 and Q78). Further downstream, the axial peak velocity gradually returns to the center of the artery. These flow features

are consistent with previous findings (Fei et al., 1994; Inzoli et al., 1996; Bertolotti and Deplano, 2000).

Comparison between the axial velocity of the Newtonian and the non-Newtonian flows reveals that the velocity profiles of the non-Newtonian flow show significant flattening, especially in the region close to the toe. The shear thinning effect of the non-Newtonian flow reduces the peak velocity of the flow where the shear rate is the lowest and increases velocity near the wall where the shear rate is high. Shift of the peak velocity toward the bottom wall is less significant for the non-Newtonian flow. This can be seen most clearly at the cross section  $x/D = 2$  when flow from the graft dominates, i.e., at Q78, where the difference in the axial velocity profiles between the non-Newtonian and the Newtonian flows is significant. The rescaled Newtonian flow, in comparison, agrees well to the non-Newtonian flow, although there are noticeable differences in the peak values of the axial velocity. These findings agree to those obtained by Gijsen et al. (1999a, b) and Chen and Lu (2004, 2005), where non-Newtonian flow in carotid bifurcation was studied.

The profiles of the axial velocity in the perpendicular plane (i.e.,  $x - y$  plane) are presented in Fig. 4. At the toe, the jet flow induces an obvious peak value of the axial velocity at the center of the artery, in particular in the case Q12 where the 50% of the total flow is from the stenosed artery. The maximum velocity decreases as the distance between the stenosis and the anastomosis increases (e.g., at D2, D3 and D0), and a typical flat

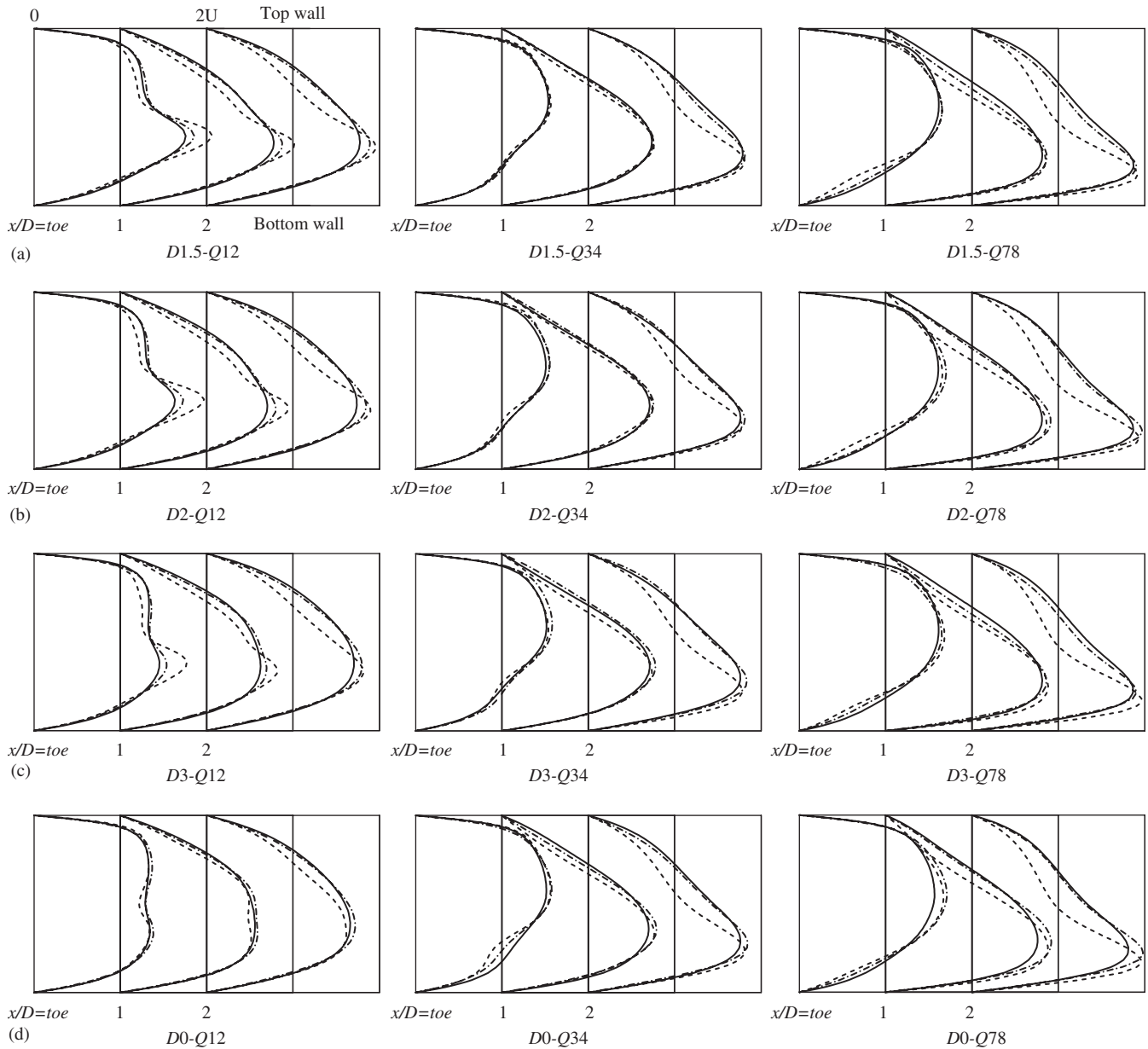


Fig. 3. Axial velocity profiles of the non-Newtonian flow (solid line), the Newtonian flow (dashed line) and the rescaled Newtonian flow (dash-dot line) in the  $x-z$  plane. The ratio between flows in the stenosed artery and in the bypass graft takes different values. (a)  $D1.5$ ; (b)  $D2$ ; (c)  $D3$ ; (d)  $D0$ .

velocity profile is found at the toe in the case  $D0-Q12$  (in Fig. 4d). The peak velocity at the toe increases as the flow rate in the bypass graft increases for both the Newtonian and the non-Newtonian flows. Downstream of the toe, typical M-shape velocity profiles are formed at  $x/D = 2$ , which are consistent with observations in abdominal aorta model and coronary artery branch by [Perktold et al. \(1998\)](#). The location of the double peaks in the M-shape velocity profile becomes closer to the lateral walls as the flow rate in the graft increases, which is similar to the findings by [Bertolotti and Deplano \(2000\)](#). The trough of the M-shape velocity profile at the center of the artery is more pronounced at higher flow

rate in the graft, caused by the stronger inertia in the flow from the graft. This feature is confirmed by the presence of stronger secondary flows in the cross-sectional plane, which will be shown later. Difference in the velocity profiles between the non-Newtonian and the Newtonian flows can be seen most clearly at the cross section,  $x/D = 2$ . The shear-thinning behavior of the non-Newtonian fluid induces flattened velocity profiles, and the typical M-shape velocity profiles become less evident. The rescaled Newtonian flow, on the other hand, produces axial velocity profiles that agree reasonably well to those of the non-Newtonian flow.

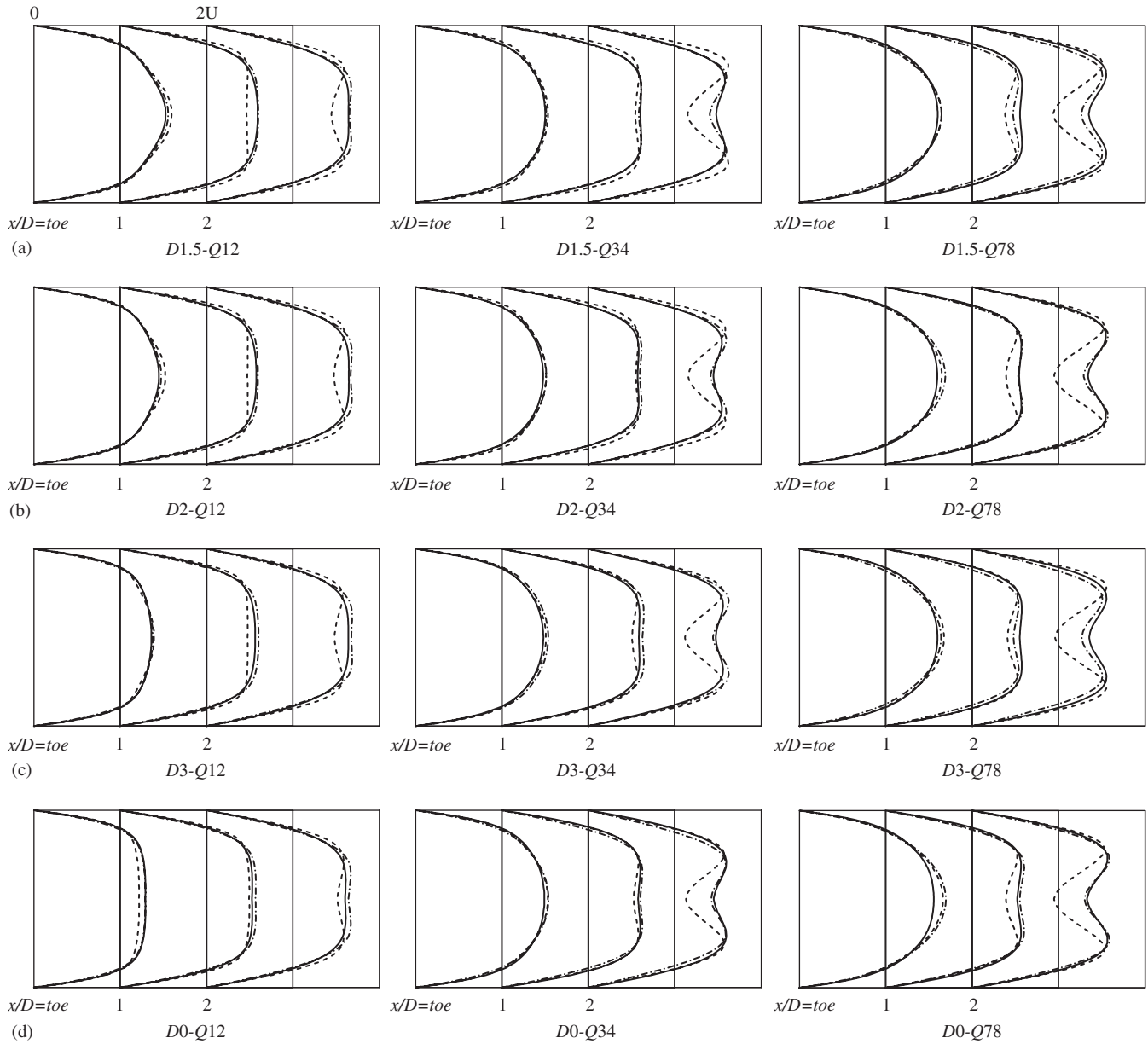


Fig. 4. Axial velocity profiles in the  $x$ – $y$  plane of the non-Newtonian flow (solid line), the Newtonian flow (dashed line) and the rescaled Newtonian flow (dash-dot line) flows. The ratio of flows in the stenosed artery and in the bypass graft takes different values. (a)  $D1.5$ ; (b)  $D2$ ; (c)  $D3$ ; (d)  $D0$ .

### 3.2. Velocity contours and secondary flow patterns

Development of the velocity with the distance in the host artery can be seen in velocity contours at different cross sections. In Fig. 5a, axial velocity contours at the toe and  $x/D = 1, 2.5$  and  $5$ , are presented for the case  $D1.5$ . In the figure, velocity contours have the same range of values in all panels for easy comparison. Interaction between the flow from the bypass graft and the jet flow from the stenosed artery is clearly illustrated in these contours. At the toe, maximum velocity becomes more and more dominated by the flow from the graft and its location shifts toward the top wall as we

move from the top panel (i.e.,  $Q12$ ) to the bottom panel (i.e.,  $Q78$ ). The crescent contours of the axial velocity emerge at  $x/D = 1$  and grow stronger at  $x/D = 2.5$ . When flow becomes more and more dominated by fluid from the bypass graft, e.g., at  $Q34$  and  $Q78$ , the crescent-shaped velocity contours become more obvious and skew closer to the bottom wall. At  $x/D = 5$ , velocity develops toward a more parabolic profile, particularly when the flow is non-Newtonian. In comparison, the crescent-shaped distortion is weaker for the non-Newtonian flow. This means that the non-Newtonian effect of the fluid weakens the secondary flows in sections downstream of the anastomosis. The

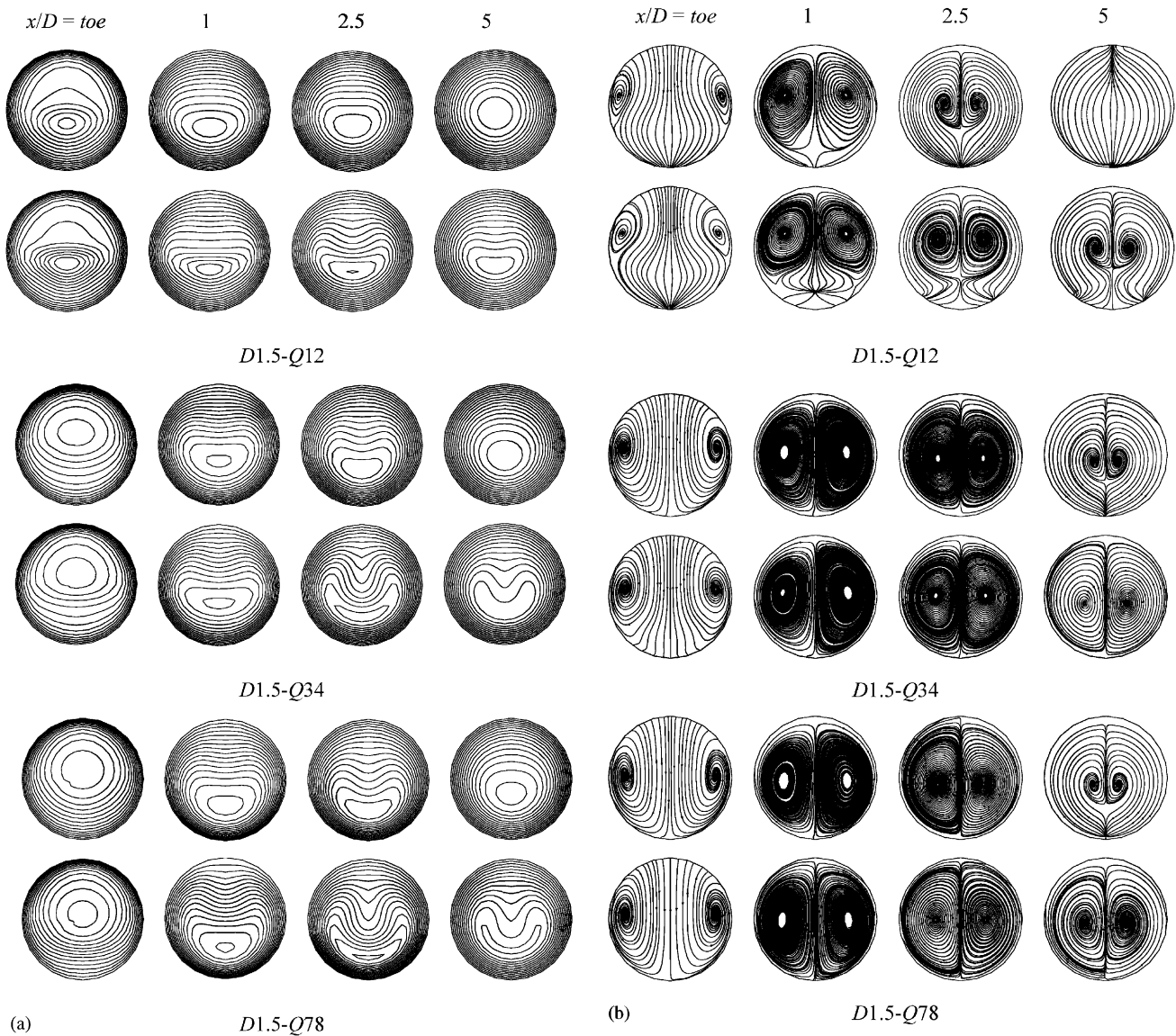


Fig. 5. Comparison between the non-Newtonian flow (top) and the Newtonian flow (bottom) at four different cross sections: at the toe and at  $x/D = 1, 2.5$  and  $5$  in the case  $D1.5$ . Flow rate in the bypass graft equals  $\frac{1}{2}$  (top panels),  $\frac{3}{4}$  (middle panels) and  $\frac{7}{8}$  (bottom panels) of the total flow rate. (a) Axial velocity contours; (b) secondary flow streamlines.

velocity contours are consistent with the axial velocity profiles in Figs. 3 and 4, where flattened velocity profiles are observed for the non-Newtonian flow due to the shear-thinning behavior of the fluid.

Secondary flow streamlines at the four cross sections are shown in Fig. 5b for the case  $D1.5$ . In the figure, streamlines have the same range of values in all panels for easy comparison. Due to the flow from the bypass graft, there are pronounced movement of fluid from the top wall toward the bottom wall in the middle of the cross section. Meanwhile, an opposite fluid motion is generated by the transverse pressure gradient, thus counter-rotating vortices (Dean vortices) are evident in sections downstream of the toe. When the flow from the

stenosed artery is strong, e.g., at  $Q12$ , the cores of the secondary counter-rotating vortices are closer to the top wall of the artery, in comparison to those when the residual flow is weak, e.g., at  $Q78$ . The difference in the location of the vortices becomes less obvious in sections far away from the toe, when the secondary flows weaken in strength along the artery and vortices move toward the center of the vessel. As the flow rate in the bypass graft increases, motions in the  $z$ -direction increase relative to the transverse ones. At  $Q78$ , fluid movement in the  $z$ -direction is of the same order as that in the  $x$ -direction, the intensity of the two symmetric vortices is the highest. Non-Newtonian fluid weakens the strength of the secondary motion of the flow in the artery in all

sections at all flow rates. This can be seen most clearly at  $x/D = 5$  at  $Q_{12}$ , where vortices are evident in Newtonian flow (bottom figure) but are absent in the corresponding non-Newtonian flow (top figure).

### 3.3. Wall shear stress (WSS)

To illustrate WSS distribution in the host artery, WSS along three lines in the artery, i.e., upstream of the junction (line  $A-A'$  in Fig. 1b), downstream of the junction (line  $B-B'$ ) and along the bottom wall (line  $C-C'$ ), are shown in Fig. 6. Significant difference in WSS between the non-Newtonian and Newtonian flows is observed at these locations. Here, the WSS is normalized by the mean WSS for Newtonian flow at the outlet of the host artery, i.e.,  $S_c = \eta(8V/D)$ , where  $\eta$  is the Newtonian viscosity,  $V$  the mean velocity at the

outlet of the host artery and  $D$  the diameter of the host artery.

In Fig. 6a, distributions of WSS along the line  $A-A'$  are given for different flow inputs and stenosis locations. When the residual flow in the stenosed artery is strongest, i.e., at  $Q_{12}$ , negative WSS exists along most part of the line when the stenosis is close to the junction, i.e., in the case  $D1.5$ . The negative value in WSS indicates flow recirculation downstream of the stenosis near the top wall. As the distance between the stenosis and the junction increases, i.e. in case  $D3$ , WSS increases. When the stenosis is far away from the junction, i.e.,  $D0$ , there is no recirculating flow near the heel of the graft and WSS is positive along  $A-A'$ . As the flow in the bypass graft becomes more dominating, i.e., at  $Q_{34}$  and  $Q_{78}$ , WSS along  $A-A'$  increases in value except in the case  $D0$ , where reduced flow rate in the stenosed artery results in lowered WSS. The

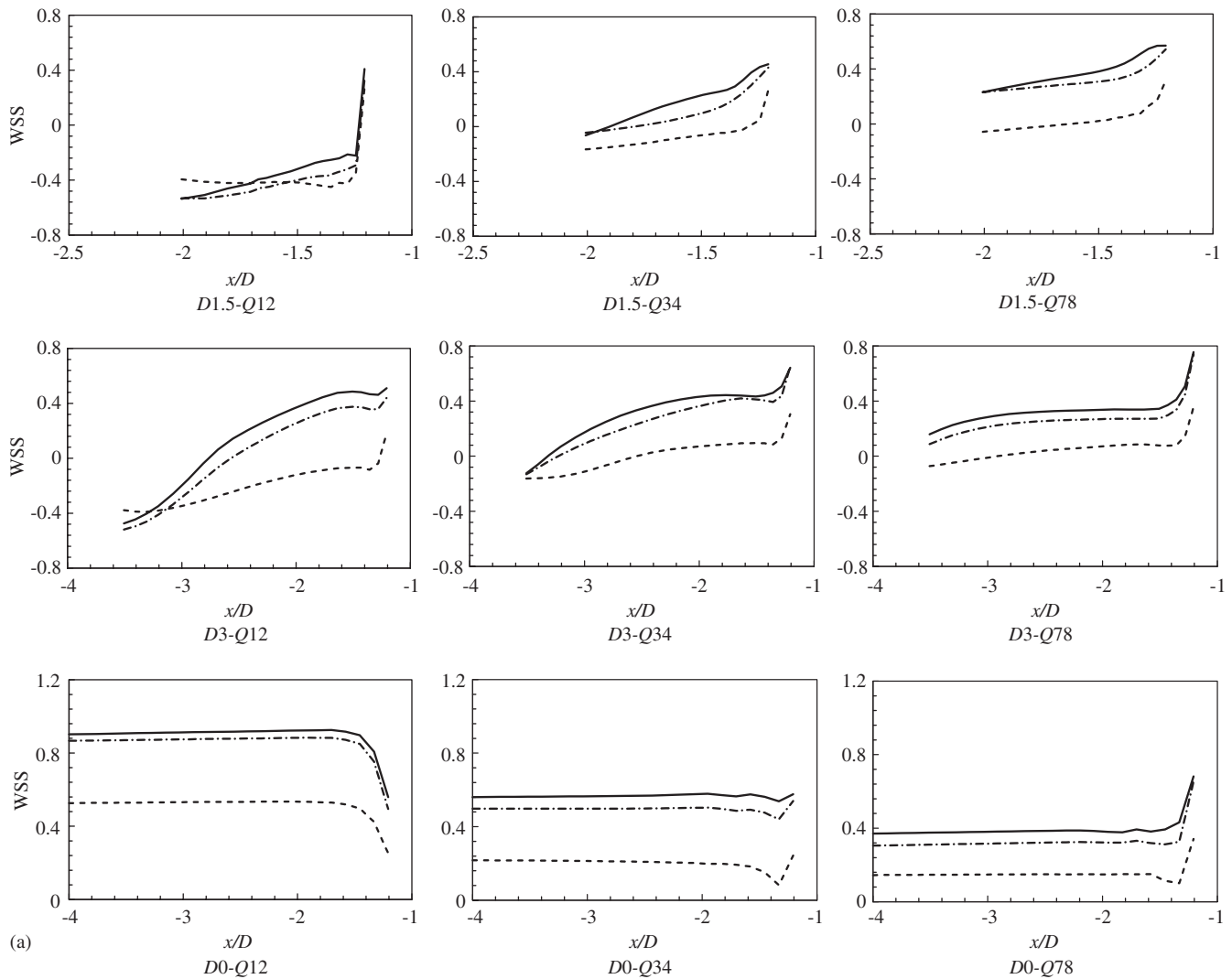


Fig. 6. Distribution of the wall shear stress of the non-Newtonian flow (solid line), the Newtonian flow (dashed line) and the rescaled Newtonian flow (dash-dot line) in the host artery. In the figure, the ratio between flows in the stenosed artery and in the bypass graft takes different values, and the distance between the graft and the stenosis varies: (a) along the line  $A-A'$ ; (b) along the line  $B-B'$ ; (c) along the line  $C-C'$ .

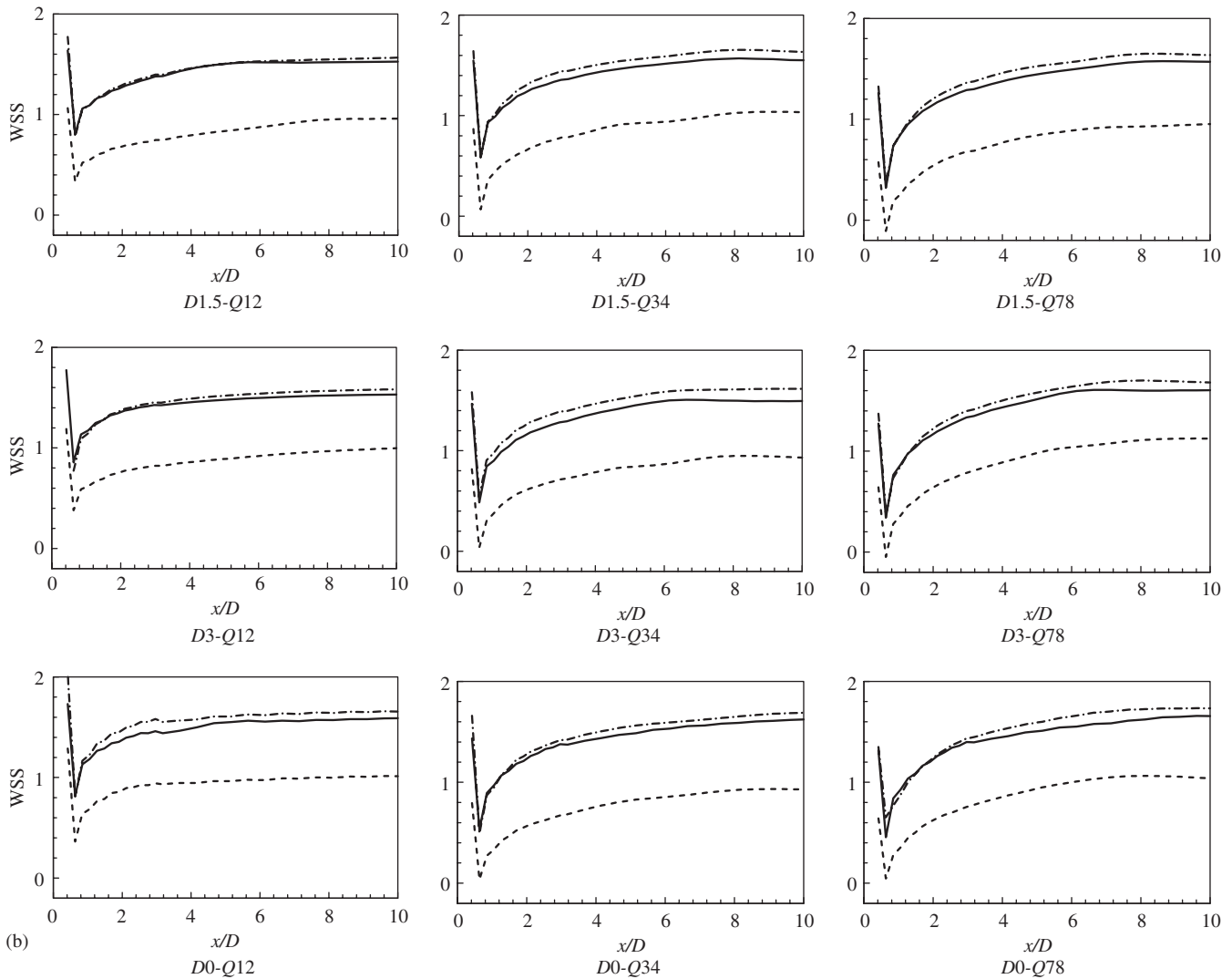


Fig. 6. (Continued)

location of the zero WSS (i.e., the stationary point on the top wall where WSS changes from negative to positive) moves toward the stenosis. The recirculating flow downstream of the stenosis becomes weaker in strength and smaller in size. Near the heel of the anastomosis, there are rapid changes in WSS in all cases. Higher values in WSS are observed for the non-Newtonian flow in all cases. In comparison to Newtonian flow, the size of the recirculating flow downstream of the stenosis is much smaller in size and much weaker in strength, as indicated by the magnitude of the negative WSS.

In Fig. 6b, distribution of WSS along the line  $B-B'$  is presented for different flow inputs and stenosis locations. Positive WSS is observed at the top wall of the artery downstream of the bypass junction. When the flow input from the stenosed artery reduces and flow is dominated by the inflow from the bypass graft, i.e., at  $Q78$ , there is a small negative WSS near the toe of the

bypass graft (for Newtonian flow only), indicating a small flow recirculating zone there. There is a sudden drop in WSS at  $x/D \approx 0.6$  where minimum WSS exists for both the Newtonian and the non-Newtonian flows. This is caused by the fact that flow there has a strong component in the transverse direction (as shown in the secondary flow streamlines in Fig. 5b) and the peak axial velocity is furthest from the top wall of the artery (as shown in axial velocity contours in Fig. 5a). Further downstream, WSS increases with distance in the flow direction and reaches a constant value when flow becomes fully developed. Non-Newtonian flow results in bigger WSS along the entire length of the line  $B-B'$  for all flow conditions studied, which can be expected from the more centrally distributed axial velocity contours (than those of the Newtonian flow) shown in Fig. 5a.

In Fig. 6c, distributions of WSS along the bottom wall (i.e., line  $C-C'$ ) are presented. In the stenosed artery,

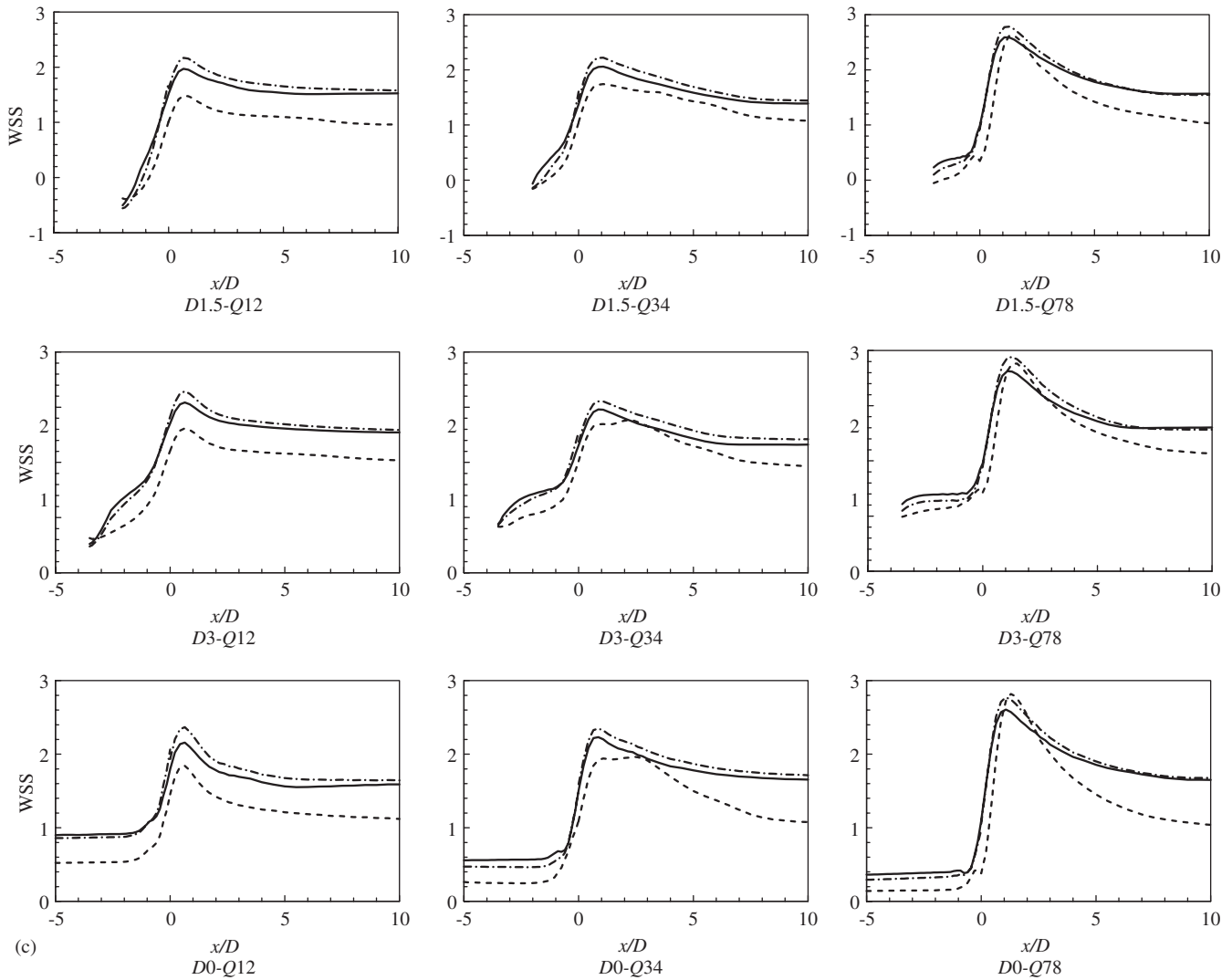


Fig. 6. (Continued)

flow recirculation downstream of the stenosis results in negative WSS (except in case *D0* where there is no stenosis and no flow recirculation occurs), which is rather similar to that observed in Fig. 6a. WSS at the bottom wall increases with the distance in the flow direction, reaching maximum at  $x/D \approx 0.6$ . This corresponds well to the minimum WSS on the top wall at the same  $x$  distance. Near the toe of the graft, there is rapid increase in the WSS which in part is due to the additional flow from the bypass graft, and in part due to the fact that flow is forced onto the bottom wall of the artery. As the flow rate in the graft increases, the peak value of WSS is higher. This character is consistent with previous findings (Fei et al., 1994; Inzoli et al., 1996; Bertolotti and Deplano, 2000). Further downstream in the artery, WSS at the bottom wall decreases gradually and reaches a constant value when fully developed flow is established. Again, WSS of the non-Newtonian flow is higher than that of the Newtonian flow. However, at

*Q78*, a lower peak WSS is observed for the non-Newtonian flow than that for the Newtonian flow. This is caused by the high flow rate in the bypass graft, which results in big shear rate at the bottom wall. The shear-thinning effect of the non-Newtonian fluid reduces the peak WSS.

To illustrate WSS distribution in the graft vessel, WSS along two lines, i.e., heel side of the graft (line *A–A'* in Fig. 1b) and toe side (line *B–B'*), are shown in Fig. 7. Velocity profiles (not shown here) in the graft vessel demonstrate typical parabolic distributions for the Newtonian, rescaled Newtonian and non-Newtonian flows. No flow recirculation is observed in the graft vessel. WSS increases rapidly near the toe region for all flow conditions. Increase in the flow rate in the graft results in higher WSS. WSS for the non-Newtonian flow is higher than that of the Newtonian flow, and the rescaled Newtonian flow gives nearly identical WSS to that of the non-Newtonian flow.

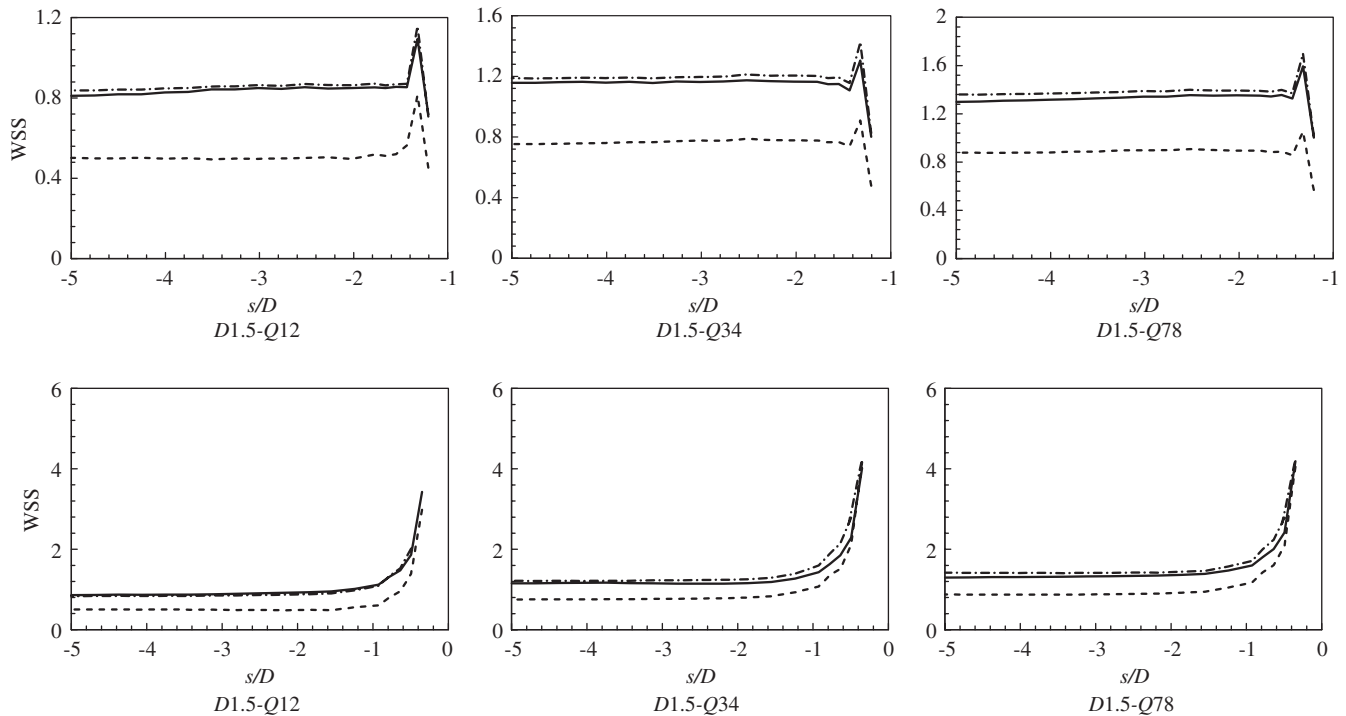


Fig. 7. Distribution of the wall shear stress along lines  $A-A'$  (top panels) and  $B-B'$  (bottom panels) in the graft vessel for the non-Newtonian flow (solid line), the Newtonian flow (dashed line) and the rescaled Newtonian flow (dash-dot line).

The agreement between WSS of the rescaled Newtonian flow and that of the non-Newtonian flow is somewhat less than satisfactory along the line  $A-A'$ . This is caused by the fact that the mean velocity used in Eq. (5) (i.e., the mean velocity at the outlet) is a poor representation of the flow in the stenosed artery. Better overall agreement is seen in the artery downstream of the junction. The rescaled Newtonian fluid, as predicted, underestimates WSS in regions with low wall shear rate and overestimates WSS in regions with high shear rate. This behavior has been confirmed by Gijsen et al. (1999a, b) and Chen and Lu (2004, 2005). The application of the rescaled Newtonian fluid is difficult to be generalized for different geometries and flow conditions; however, it is noted that the WSS predicted by the rescaled Newtonian flow is reasonably consistent with that of the non-Newtonian flow along lines  $B-B'$  and  $C-C'$  in the host artery as well as along lines  $A-A'$  and  $B-B'$  in the graft.

#### 4. Discussion

Arterial diseases tend to develop in regions with flow separation, recirculation, low and oscillating WSSs, which are believed to be atheromatic factors (Giddens et al., 1976; Araim et al., 2001). Once plaque develops and encroaches into the lumen, further flow disturbances are

inevitable (Ku, 1997). There is increasing interest in analyzing the stresses and flow patterns in stenosed coronary bypasses due to thrombosis and anastomotic intimal hyperplasia following coronary bypass surgeries. In the present study, primary and secondary flows and WSS distribution in a stenosed artery are calculated with different distances of grafting and different ratios between flows from the graft and the stenosed artery. The axial velocity profiles are seen to skew toward the opposite wall to the anastomosis and counter-rotating vortices (Dean vortices) are formed downstream of the junction. High values of the WSS appear at the opposite wall to the anastomosis near the junction, where flow from the graft impacts on the arterial wall. Due to the shear-thinning effect of the non-Newtonian flow, the axial velocity profiles are flattened and the secondary flows (i.e., counter-rotating vortices) are weakened in the artery. Flow recirculation occurs downstream of the stenosis and near the toe of the graft. The strength of the recirculating flow and the size of the recirculation zone are significantly reduced when the non-Newtonian behavior of the blood is considered.

The residual flow from the stenosed artery interacts with the flow from the graft and contributes to overall velocity and WSS distribution near the junction. As the flow rate in the stenosed artery decreases following surgery, the residence time for atherogenic particles (e.g., platelets and macrophages) in the stenosed artery

increases, promoting the deposition and adhesion of the particles in the diseased artery (Caro et al., 1971). Flow from the bypass graft introduces secondary motions in the artery. Near the toe of the graft, there are steep variations in the WSS at both the top wall and the bottom wall of the artery, which may correlate to the occurrence of hyperplasia downstream of the toe. The high values of WSS at the opposite wall to the anastomosis may induce platelet activation and aggregation (Worthley et al., 2001). The distance between the graft and the stenosis is seen to affect flow and WSS distribution at the junction and downstream sections. As the distance increases, the jet flow over the stenosis dissipates before it reaches the junction. Flow recirculation stops short of the heel of the graft, minimizing risks of intimal hyperplasia at the anastomosis. Flow structures, pressure and WSS distribution have an important effect on the suture-line, where the compliance mismatch between the graft and the host artery is a source of failure of the bypass grafting. Interaction between flows from the graft and the stenosed artery results in steep variations in the WSS near the heel and the toe of the graph (seen in Figs. 6a and 6b). When combined with flow recirculation near these regions, they facilitate intimal proliferation and thrombogenesis near the suture-line.

Arterial flow and WSS distribution are strongly affected by rheological properties of the blood. Significant differences in velocity profiles, secondary flow patterns and WSS distributions are seen between the Newtonian and the non-Newtonian flows in the study. The shear thinning behavior of the blood allows for approximation using a rescaled viscosity based on a characteristic shear rate of the flow. However, there is no universally accepted definition of the characteristic shear rate, and inconsistency between the rescaled Newtonian flow and the non-Newtonian flow is inevitable regardless of the choice of the characteristic shear rate. In the present study, the averaged shear rate based on the mean arterial velocity at the outlet is used. The rescaled Newtonian flow is found to give reasonable representation of the non-Newtonian flow in most situations. The non-Newtonian behavior of the blood also introduces differences in the flow field of the blood in different age populations. In elderly people, the characteristic shear rate is lower and the rescaled viscosity is therefore higher (Reneman et al., 1985). The opposite occurs in young people, where blood behaves more like a Newtonian fluid due to higher characteristic shear rate in the circulation.

In conclusion, non-Newtonian behavior of the blood is a key factor affecting the primary and secondary flow patterns near the junction between the bypass graft and the stenosed artery. The WSS values and distributions are also significantly altered. It is, therefore, essential to take into consideration of the non-Newtonian effect of

the blood, when the relationship between hemodynamic factors of the blood circulation and vascular diseases is investigated. A simple Newtonian fluid model for the blood may lead to false interpretation of experimental observations, particularly when complex vascular geometries are considered, e.g., near arterial bypass grafts, where the shear thinning effect of the blood may result in much reduced flow recirculation and vortices in the blood stream.

### Acknowledgments

The authors thank Professor L.-X. Zhuang for helpful discussions. The study was supported by the Chinese Academy of Sciences (Outstanding Overseas Chinese Scholars Fund and the Hundred Talent Program) and the National Natural Science Foundation (No. 10028205).

### References

- Araim, O., Chen, A.H., Sumpio, B., 2001. Hemodynamic forces: effects on atherosclerosis. *New Surgery* 1, 92–100.
- Baaijens, J.P.W., van Steenhoven, A.A., Janssen, J.D., 1993. Numerical analysis of steady generalized Newtonian flow in a 2D model of the carotid artery bifurcation. *Biorheology* 30, 63–74.
- Ballyk, P.D., Steinman, D.A., Ethier, C.R., 1994. Simulation of non-Newtonian blood flow in an end-to-side anastomosis. *Biorheology* 31, 565–586.
- Bertolotti, C., Deplano, V., 2000. Three-dimensional numerical simulations of flow through a stenosed coronary bypass. *Journal of Biomechanics* 33, 1011–1022.
- Bertolotti, C., Deplano, V., Fuseri, J., Dupouy, P., 2001. Numerical and experimental models of post-operative realistic flows in stenosed coronary bypasses. *Journal of Biomechanics* 34, 1049–1064.
- Bird, R.B., Armstrong, R.C., Hassager, O., 1987. , second ed. *Dynamics of Polymer Liquids*, vol. 1. Wiley, New York.
- Caro, C.G., Baker, A.J., Fitzgerald, J.M., Schroter, R.C., 1971. Atheroma and arterial wall shear: observations, correlation and proposal of a shear dependent mass transfer mechanism for atherogenesis. *Proceedings of the Royal Society of London B* 117, 109–159.
- Chen, J., Lu, X.Y., 2004. Numerical investigation of the non-Newtonian blood flow in a bifurcation model with a non-planar branch. *Journal of Biomechanics* 37, 1899–1911.
- Chen, J., Lu, X.Y., 2005. Numerical investigation of the non-Newtonian pulsatile blood flow in a bifurcation model with a non-planar branch. *Journal of Biomechanics*, in press, online available.
- Chien, S., Usami, S., Dellenback, R.J., Gregersen, M.I., 1970. Shear dependent deformation of erythrocytes in rheology of human blood. *American Journal of Physiology* 219, 136–142.
- Cho, Y.I., Kensey, R., 1991. Effects of the non-Newtonian viscosity of blood flows in a diseased arterial vessel. Part 1: steady flows. *Biorheology* 28, 241–262.
- Cole, J.S., Gillan, M.A., Raghunathan, S., O'Reilly, M.J.G., 1998. Numerical simulations of time-dependent non Newtonian blood flow through typical human arterial bypass grafts. *Sixth Irish Chemical Engineering Research Symposium*, Cork.

- Crawshaw, H.M., Quist, W.C., Serrallach, E., Valeri, R., Logerfo, F.W., 1980. Flow disturbance at the distal end-to-side anastomosis. *Archives of Surgery* 115, 1280–1284.
- Ethier, C.R., Steinman, D.A., Zhang, X., Karpik, S.R., Ojha, M., 1998. Flow waveform effects on end to side anastomotic flow patterns. *Journal of Biomechanics* 31, 609–617.
- Fei, D.Y., Thomas, J.D., Rittgers, S.E., 1994. The effect of angle and flow rate upon hemodynamics in distal vascular graft anastomoses: a numerical study. *Journal of Biomechanical Engineering* 116, 331–336.
- Friedman, M.H., Ding, Z.H., 1998. Variability of the planarity of the human aortic bifurcation. *Medical Engineering and Physics* 20, 469–472.
- Friedman, M.H., Peters, O.J., Barger, C.B., Hutchins, G.M., Mark, F.F., 1981. Correlation between intimal thickness and fluid shear in human arteries. *Atherosclerosis* 39, 425–436.
- Giddens, D.P., Mabon, R.F., Cassanova, R.A., 1976. Measurements of disordered flows distal to subtotal vascular stenoses in the thoracic aortas of dogs. *Circulation Research* 39, 112–119.
- Gijzen, F.J.H., van de Vosse, F.N., Janssen, J.D., 1999a. The influence of the non-Newtonian properties of blood on the flow in large arteries: steady flow in a carotid bifurcation model. *Journal of Biomechanics* 32, 601–608.
- Gijzen, F.J.H., van de Vosse, F.N., Janssen, J.D., 1999b. The influence of the non-Newtonian properties of blood on the flow in large arteries: unsteady flow in a 90° curved tube. *Journal of Biomechanics* 32, 705–713.
- Henry, F.S., Collins, M.W., Hughes, P.E., How, T.V., 1996. Numerical investigation of steady flow in proximal and distal end-to-side anastomoses. *Journal of Biomechanical Engineering* 118, 302–310.
- Hofer, M., Rappitsch, G., Perktold, K., Turbel, W., Schima, H., 1996. Numerical study of wall mechanics and fluid dynamics in end-to-side anastomoses and correlation to intimal hyperplasia. *Journal of Biomechanics* 29, 1297–1308.
- Imparato, A.M., Bracco, A., Kim, G.E., Zeff, R., 1972. Intimal and neointimal fibrous proliferation causing failure of arterial reconstructions. *Surgery* 72, 1007–1017.
- Inzoli, F., Migliavacca, F., Pennati, G., 1996. Numerical analysis of steady flow in aorto-coronary bypass 3-D model. *Journal of Biomechanical Engineering* 118, 172–179.
- Kakos, G.S., Oldham, H.N., Dixon, S.H., Davis, R.W., Hagen, P.-O., Sabiston Jr., D.C., 1972. Coronary artery hemodynamics after aorto-coronary artery vein bypass. *Journal of Thoracic and Cardiovascular Surgery* 63, 849–853.
- Keynton, R.S., Rittgers, S.E., Shu, M.C., 1991. The effect of angle and flow rate upon hemodynamics in distal vascular graft anastomoses: an in vitro model study. *Journal of Biomechanical Engineering* 113, 458–463.
- Kovacs, A., Kawahara, M., 1991. A finite element scheme based on the velocity correction method for the solution of the time-dependent incompressible Navier–Stokes equations. *International Journal for Numerical Methods in Fluids* 13, 403–423.
- Ku, D.N., 1997. Blood flow in arteries. *Annual Review of Fluid Mechanics* 29, 399–434.
- Ku, D.N., Liepsch, D., 1986. The effect of non-Newtonian viscoelasticity and wall elasticity on flow at a 90° bifurcation. *Biorheology* 23, 359–370.
- Lee, D., Su, J.M., Liang, H.Y., 2001. A numerical simulation of steady flow fields in a bypass tube. *Journal of Biomechanics* 34, 1407–1416.
- Liepsch, D., Moravec, S., 1984. Pulsatile flow of non-Newtonian fluid in distensible models of human arteries. *Biorheology* 21, 571–586.
- Lou, Z., Yang, W.J., 1993. A computer simulation of the non-Newtonian blood flow at the aortic bifurcation. *Journal of Biomechanics* 26, 37–49.
- Lu, Y.L., Lu, X.Y., Zhuang, L.X., Wang, W., 2002. Breaking symmetry in non-planar bifurcation: distribution of flow and wall shear stress. *Biorheology* 39, 431–436.
- Mann, D.E., Tarbell, J.M., 1990. Flow of non-Newtonian blood analog fluids in rigid curved and straight artery models. *Biorheology* 27, 711–733.
- Nerem, R.M., 1992. Vascular fluid mechanics, the arterial wall, and atherosclerosis. *Journal of Biomechanical Engineering* 114, 274–282.
- Ofili, E.O., Kern, M.J., St. Vrain, J.A., Donohue, T.J., Bach, R., Al-Joundi, B., Aguirre, F.V., Castello, R., Labovitz, A.J., 1995. Differential characterization of blood flow, velocity, and vascular resistance between proximal and distal normal epicardial human coronary arteries: analysis by intracoronary Doppler spectral flow velocity. *American Heart Journal* 130, 37–46.
- Perktold, K., Hofer, M., Rappitsch, G., Loew, M., Kuban, B.D., Friedman, M.H., 1998. Validated computation of physiologic flow in a realistic coronary artery branch. *Journal of Biomechanics* 31, 217–228.
- Reneman, R.S., van Merode, T., Hick, P., Hoeks, A.P.G., 1985. Flow velocity patterns in and distensibility of the carotid artery bulb in subjects of various ages. *Circulation* 71, 500–509.
- Rittgers, S.E., Karayannacos, P.E., Guy, J.F., Nerem, R.M., Shaw, G.M., Hostetler, J.R., Vasko, J.S., 1978. Velocity distribution and intimal proliferation in autologous vein grafts in dogs. *Circulation Research* 42, 792–801.
- Santamarina, A., Weydahl, E., Siegel Jr., J.M., Moore Jr., J.E., 1998. Computational analysis of flow in a curved tube model of the coronary arteries: effects of time-varying curvature. *Annals of Biomedical Engineering* 26, 944–954.
- Siouff, M., Deplano, V., Pélissier, R., 1998. Experimental analysis of unsteady flows through a stenosis. *Journal of Biomechanics* 31, 11–19.
- Sottiriuri, V.S., Yao, J.S.T., Batson, R.C., Sue, S.L., Jones, R., Nakamura, Y.A., 1989. Distal anastomotic intimal hyperplasia: histopathological character and biogenesis. *Annals of Vascular Surgery* 1, 26–33.
- Thurston, G.B., 1973. Frequency and shear rate dependence of viscoelasticity of human blood. *Biorheology* 10, 375–381.
- Thurston, G.B., 1979. Rheological parameters for the viscosity, viscoelasticity and thixotropy of blood. *Biorheology* 16, 149–162.
- Tu, C., Deville, M., 1996. Pulsatile flow of non-Newtonian fluids through arterial stenoses. *Journal of Biomechanics* 29, 899–908.
- Weydahl, E.S., Moore Jr., J.E., 2001. Dynamic curvature strongly affects wall shear rates in a coronary artery bifurcation model. *Journal of Biomechanics* 34, 1189–1196.
- Worthley, S.G., Osende, J.I., Helft, G., 2001. Coronary artery disease: pathogenesis and acute coronary syndromes. *The Mount Sinai Journal of Medicine* 68, 167–181.
- Zarins, C.K., Giddens, D.P., Bharadvaj, B.K., Sottiriuri, V., Mabon, R.F., Glagov, S., 1983. Carotid bifurcation atherosclerosis: quantitative correlation of plaque localization with flow velocity profiles and wall shear stress. *Circulation Research* 53, 502–514.